Hindawi
Discrete Dynamics in Nature and Society
Volume 2022, Article ID 6260916, 7 pages
https://doi.org/10.1155/2022/6260916

Research Article

Miniaturized Multiband Bandpass Filters Based on a Single Multimode Resonator Loading Branches

Jie Luo[1], **Kaibo Shi**[1] **and Shanshan Gao**[1,2]

[1]*School of Information Science and Engineering, Chengdu University, Chengdu, Sichuan 610106, China*
[2]*State Key Laboratory of Millimeter Waves, Nanjing 210096, China*

Correspondence should be addressed to Jie Luo; luojie01@cdu.edu.cn

Received 28 July 2022; Accepted 27 September 2022; Published 10 October 2022

Academic Editor: Zi-Peng Wang

In this paper, the operating mechanism of proposed bandpass filters with a single multimode resonator loaded with branches is introduced. Based on the design procedure, the center frequencies of the proposed bandpass filters can be controlled due to the design freedom. Meanwhile, the proposed bandpass filters (BPFs) feature compact sizes and small insertion loss. To validate the design and analysis, a prototype was fabricated and measured with six passbands centered at 1.23/1.76/2.38/4.24/5.23/6.75 GHz. The measured result of the fabricated filter agrees well with the simulation, which indicates that the proposed structure can serve as a potential candidate for multiband BPF designs.

1. Introduction

In the modern multiservice wireless communication system, developments in microwave multiband bandpass filters (BPFs) have been gaining much attention for such as GPS, WLAN, WiMAX, and RFID applications.

In the past, some research was conducted for the design of multiband BPFs. In [1–6], different quad-band BPFs were realized based on different approaches, Yan et al. used two sets of short-stub-loaded E-Type resonators in [1], Bukuru et al. investigated quad-mode stepped impedance resonator (QMSIR) in [2], Li et al. realized novel quad-band bandpass filters on a basis of the multimode resonator (MMR) using SIRs loaded tapered-line (SIRTL) in [3], Kamma et al. used T-shaped stubs loaded with a modified ring resonator (MRR) in [4], Zhang et al. investigated three-layer stacked structures in [5], Li et al. used two-/tri-section SIRs and stepped impedance inverters in [6]. And in [7–9], some quint-band BPFs were achieved using different structures, in [7], W.Yang used multimode resonators, Liu et al. investigated uniform impedance resonators (UIRs) in [8], Hsu et al. realized a quint-band BPF using five tri-mode stub-loaded SIRs in [9]. It is noted that some works were reported for the case of sext-band application in [10–12], Chen used six pairs of semilumped resonators to achieve a sext-band BPF in [10], Hsu et al. used stepped-impedance resonators in [11], and Ai et al. used a single multimode resonator in [12]. Besides, it is still a challenge to achieve high-performance multiband BPFs with compact size, closely spaced passbands, low insertion loss, high return loss, and sharp skirt to satisfy the whole wireless communication system application demands.

In this paper, miniaturized multiband bandpass filters using a single multimode resonator loaded with branches are proposed. To validate the design and analysis, a prototype filter has been fabricated with six passbands centered at 1.23 GHz for GPS, 1.76 GHz for GSM, 2.38/5.23 GHz for WiFi, 4.23 GHz for digital relay system, and 6.75 GHz for RF. The proposed filter has a compact size, low insertion loss, and adjustable frequency response.

2. Filter, Design, and Procedure

What is shown in Figure 1 should be given here. As shown in Figure 1, θ_j ($j = 1,\ p_1,\ p_2$) corresponds to the equivalent electrical length of the microstrip line, while the characteristic impedance of the microstrip line is represented by Z_i ($i = 1,\ p_1,\ p_2$). Explain first the reason, then, give the

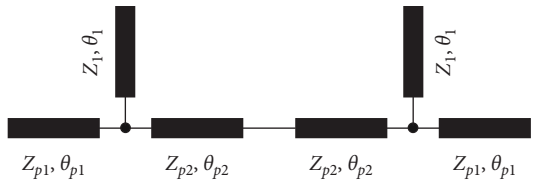

FIGURE 1: The proposed symmetrical branch loaded resonator.

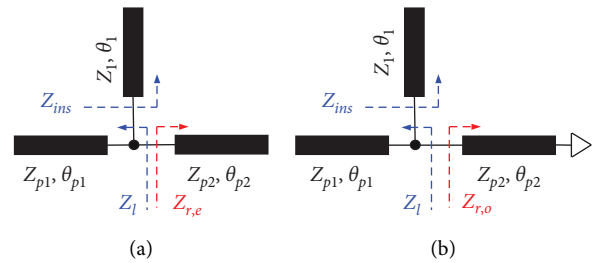

FIGURE 2: Symmetrical branch resonator equivalent circuit. (a) Even mode circuit; (b) odd mode circuit.

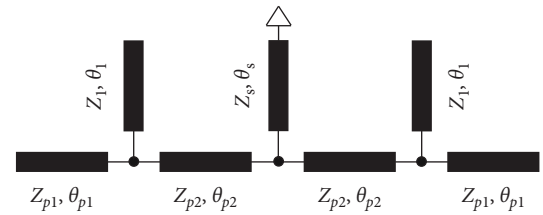

FIGURE 3: The proposed equivalent model of symmetrical branch loaded resonator.

conclusion ⟶ By increasing the length of the open branch (Z_1, θ_1), more transmission zeros can be obtained within the specified frequency range, and these transmission zeros can be used to realize the multifrequency response of the BPFs.

The characteristics of multimode resonators are analyzed by the odd and even mode method. Figure 2(a) shows the even mode equivalent circuit of symmetrical branch loaded resonators, while the odd mode equivalent circuit of symmetrical branch loaded resonators is shown in Figure 2(b). Since the transmission zeros are produced when the resonance frequencies satisfy the transverse resonance condition, the symmetrical branch-loaded resonator needs to satisfy the following formula:

$$\begin{aligned} &\mathrm{Im}\left(Z_l + Z_{r,e}\right) = 0, \\ &\mathrm{Im}\left(Z_l + Z_{r,o}\right) = 0, \\ &Z_l = \frac{Z_{\mathrm{p1}} Z_{\mathrm{ins}} \cot\theta_{\mathrm{p1}}}{jZ_{\mathrm{ins}} + Z_{p1}\cot\theta_{p1}}, Z_{\mathrm{ins}} = -jZ_1 \cot\theta_1, \\ &Z_{r,e} = -jZ_{p2}\cot\left(\theta_{p2}\right), Z_{r,o} = jZ_{p2}\tan\left(\theta_{p2}\right). \end{aligned} \tag{1}$$

When the open branch (Z_1, θ_1) port produces a virtual ground effect, the input impedance can meet the condition $Z_{\mathrm{ins}} = 0$. As a result, a set of out-of-band transmission zeros can be obtained because the signals at the input end cannot be directly transmitted to the output port and the signals are all reflected. The positions of these transmission zeros can be calculated by (2). By adjusting the out-of-band transmission zeros f_{zs} of the BPF, the required number of passbands can be obtained within a specified frequency range.

$$\begin{aligned} &\cot\theta_1 = 0, \\ &f_{\mathrm{zs}} = \frac{n\pi f_0}{2\theta_1},\ n = 1, 3, 5.... \end{aligned} \tag{2}$$

Figure 3 presents the equivalent model of the symmetrical branch loaded resonator proposed in this paper. Compared with Figure 1, a short-circuit branch (Z_s, θ_s) is introduced in the middle of the resonator with the purpose of improving the S parameter of the multiband BPFs.

By adjusting the characteristic impedance and electrical length of the microstrip line, three passbands of the BPF are generated in the range of [0, 7 GHz] through three groups of resonance points of even mode and odd mode: the first passband is composed of the fundamental resonance frequency f_{o1} and f_{e1}, the second passband is composed of the first harmonic resonance frequency f_{o2} and f_{e2}, and the third passband is composed of the first harmonic resonance frequency f_{o3} and f_{e3}.

Figure 4 shows the based tri-band equivalent transmission line model for the proposed BPF. It consists of transmission branches (Z_{p1}, θ_{p1}) (Z_{p2}, θ_{p2}), an open branch (Z_1, θ_1), and a short branch (Z_s, θ_s). The proposed BPF shown in Figure 4 can generate three passbands. The center frequencies of the three passbands are represented by f_1, f_2, and f_3, respectively. L_s represent the length of the short branch (Z_s, θ_s). It can be seen in Figure 5 that f_{e1}, f_{e2}, and f_{e3} all move to the lower frequency band with the increase of parameter L_s, while the positions of f_{o1}, f_{o2}, and f_{o3} remain unchanged, the passband bandwidth can be changed by adjusting parameter L_s.

Similarly, in Figure 5(b), L_1 represents the length of the open branch (Z_1, θ_1). L_1 is adjusted to get the center frequency variation shown in Figure 5(b). With the increase of L_1, f_{o1}, f_{o2}, f_{o3}, f_{e1}, f_{e2}, and f_{e3} all move to the lower frequency. The f_{o3} and f_{e3} in the higher frequency move to the lower frequency faster than other resonance frequencies. The center frequency can be adjusted by the fact that the resonance frequency moves at different rates with the change of L_1. To validate the proposed design flow, an example tri-band BPF is fabricated. As shown in Figure 6, the measured performances show good agreement with the simulated ones.

By increasing the number of symmetric open branches, multiple sets of fundamental and higher harmonics can be superimposed. The proposed quad-band multimode resonator based on the asymmetric tree structure is composed of an open branch (Z_2, θ_2) cascaded in the previous tri-band multimode resonator filter, as shown in Figure 7.

As shown in Figure 8, when the multimode resonator has only the open stub1, the length of the open stub1 can be adjusted to obtain a fundamental resonance at

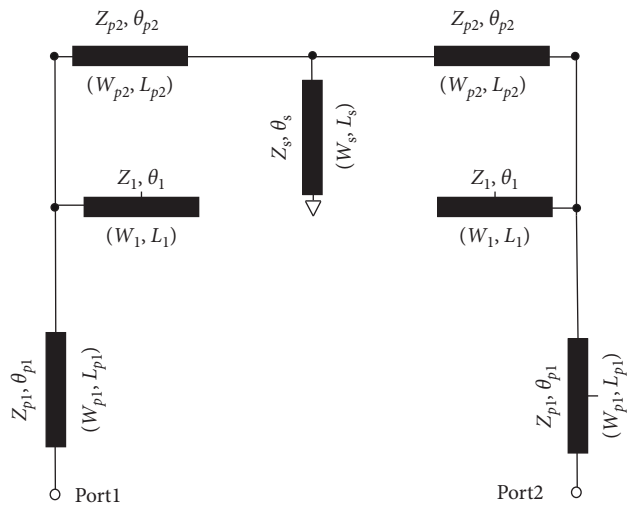

Figure 4: The based tri-band equivalent transmission line model for the proposed BPF.

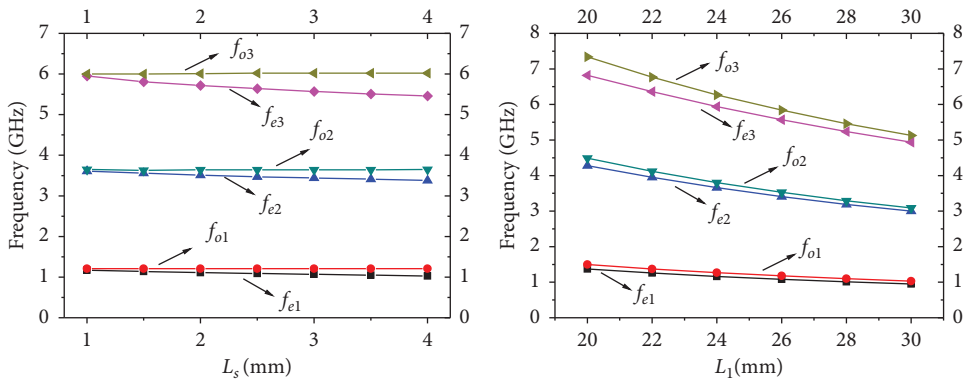

Figure 5: Variation of frequency with different L_s and L_1.

1.71 GHz and the center frequency of the first harmonic passband at 5.14 GHz. When the multimode resonator has only the open stub2, the length of the open stub2 can be adjusted to obtain a fundamental resonance at 2.19 GHz and the center frequency of the first harmonic passband at 6.44 GHz. When the multimode resonator includes both the stub1 and the stub2, the four passband center frequencies are 1.61 GHz, 2.37 GHz, 5.15 GHz, and 6.87 GHz.

To validate the proposed design flow, an example quad-band BPF is fabricated. As shown in Figure 9, good agreements between the measured and simulated performances are also observed.

From the previous theoretical analysis, it can be concluded that the obtained design method of the multiband BPFs is based on the coupling of fundamental and high-order harmonics of different branches. For example, the quad-band BPF is realized by the dual-band generated by stub1 and the other dual-band generated by stub2. If stub1 is used to realize tri-band and stub2 is used to realize dual-band, the quint-band multimode resonator can be obtained as the model shown in Figure 10.

Similarly, as shown in Figure 11, when the multimode resonator has only stub1, adjusting the length of stub1 can achieve the fundamental passband centered at 1.32 GHz, the first harmonic passband centered at 4.01 GHz, and the second harmonic passband centered at 6.54 GHz. If there is only stub2 in the multimode resonator, adjusting the length of stub2 can obtain the fundamental passband centered at 1.71 GHz and the first harmonic passband centered at 5.14 GHz. When the multimode resonator includes both stub1 and stub2, the center frequencies of the five passbands are 1.27 GHz, 1.80 GHz, 4.01 GHz, 5.31 GHz, and 6.82 GHz.

As shown in Figure 12, an example quint- band BPF is fabricated, the measurement performances show good agreements with the simulation.

Finally, the sext-band multimode resonator based on the proposed asymmetric tree structure is composed of an

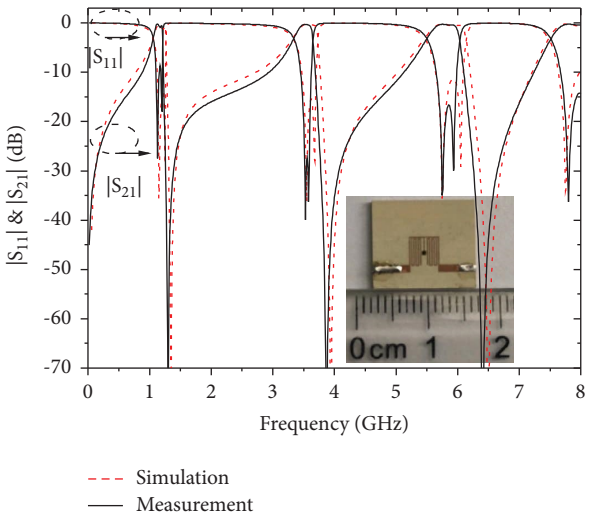

Figure 6: Simulated and measured results of tri-band BPF.

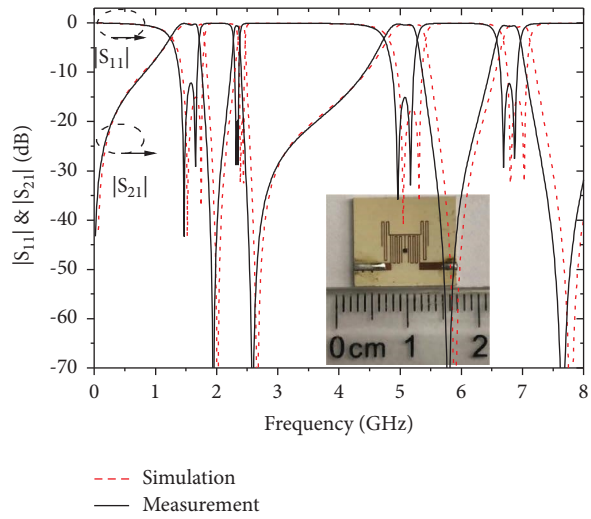

Figure 9: Simulated and measured results of quad-band BPF.

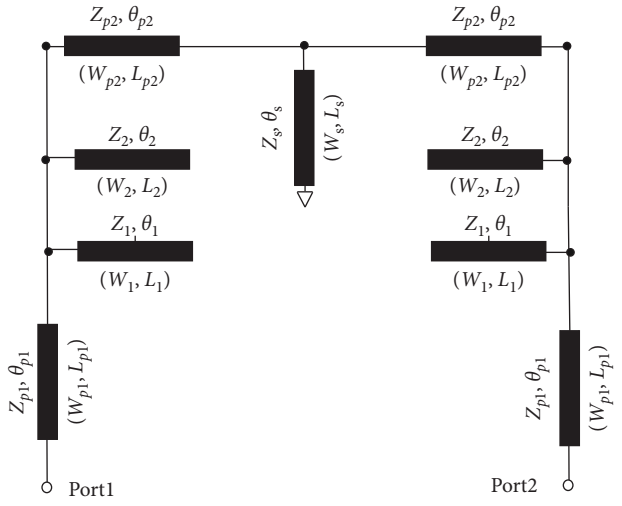

Figure 7: The quad-band equivalent transmission line model for the proposed BPF.

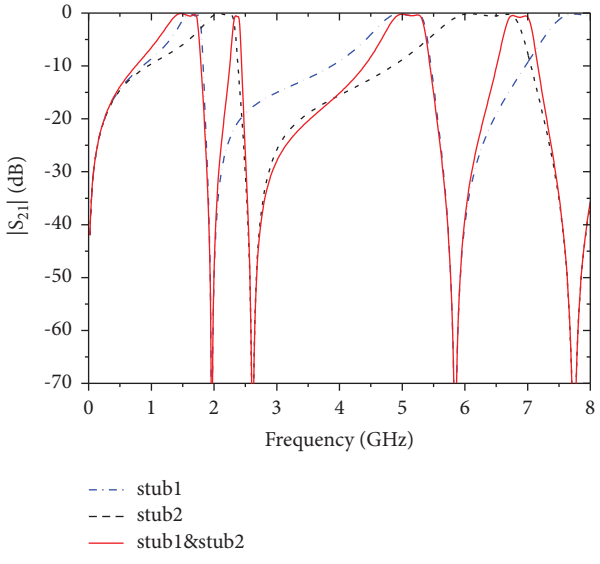

Figure 8: The $|S_{11}|$ of the proposed BPF composed of stub1 and stub2.

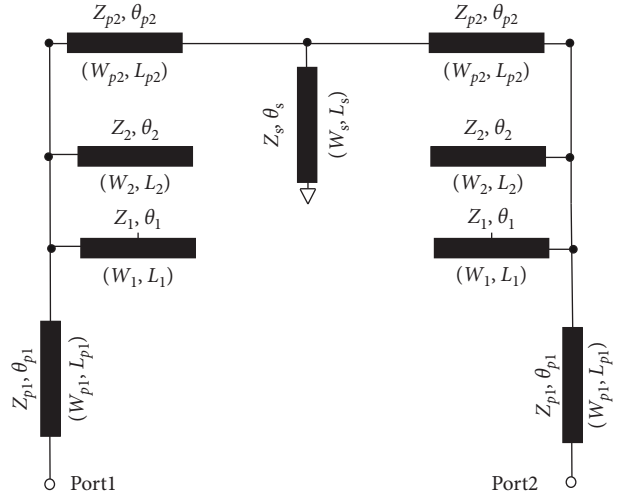

Figure 10: The quint-band equivalent transmission line model for the proposed BPF.

open branch (Z_3, θ_3) cascaded in the previous quint-band multimode resonator filter, as shown in Figure 13.

3. Results and Comparisons

The structure of the proposed sext-band BPF is shown in Figure 14. An example sext-band BPF is fabricated on a Rogers TMM10 (relative dielectric constant $\varepsilon_r = 9.20$, loss tangent $\tan\delta = 0.0022$) substrate with a thickness of 1.00 mm, as shown in the inset of Figure 12. The dimension values are summarized as follows (all in mm): $L_1 = 16.73$, $L_2 = 12.57$, $L_3 = 21.10$, $L_{p1} = 4.01$, $L_{p2} = 1.99$, $L_s = 2.01$, $W = 0.10$ mm. The overall size of the circuit is approximately $0.08\lambda_g \times 0.07\lambda_g$, where λ_g represents the guided wavelength at the first passband.

Measurement of the fabricated filter is performed using an Agilent E8363 B network analyzer. Figure 15 shows the simulated and measured S-parameters of the sext-band BPF,

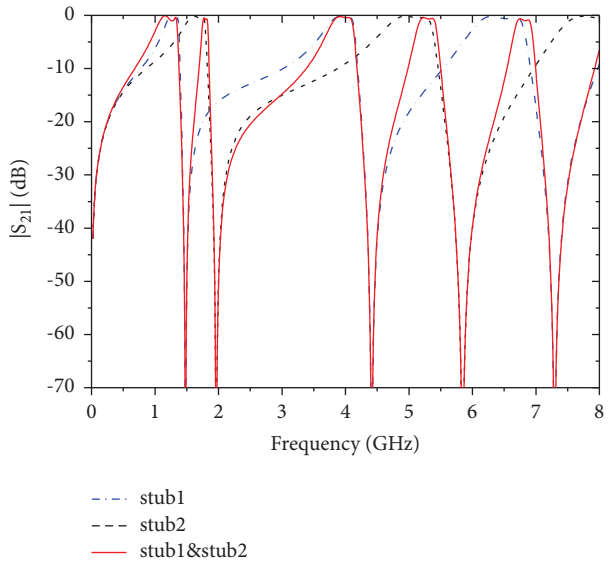

Figure 11: The $|S_{11}|$ of the proposed BPF composed of stub1 and stub2.

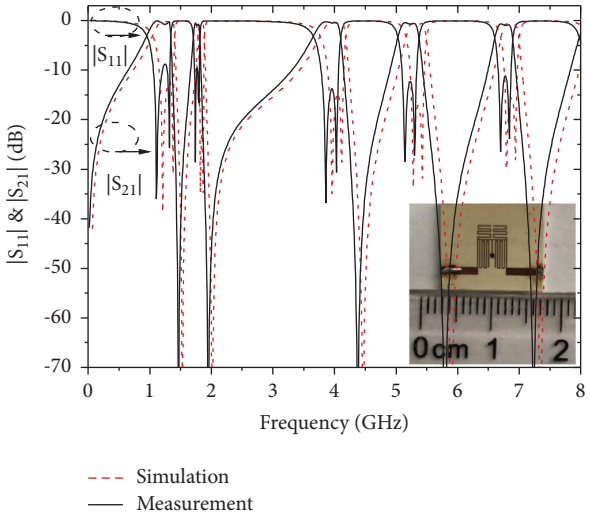

Figure 12: Simulated and measured results of quint-band BPF.

and the photograph of the fabricated BPF is also demonstrated in the inset of Figure 15. The measured six passbands are centered at 1.23/1.76/2.38/4.24/5.23/6.75 GHz with 3 dB fractional bandwidth of 29.27%/3.41%/3.78%/5.19%/3.06%/4.45%. The minimum insertion losses of each band are 1.52/1.61/1.43/0.79/0.68/0.87dB.

The band-to-band isolations are above 70 dB, which generates sharp and deep rejections between the adjacent passbands.

The slight difference between the measured and simulated results may result from the nonuniformity of the relative permittivity of the substrate, the fabrication tolerance, and SMA connectors.

In order to better evaluate the achieved performance, Table 1 presents a performance comparison of the proposed sext-band BPF with some previously reported works. The

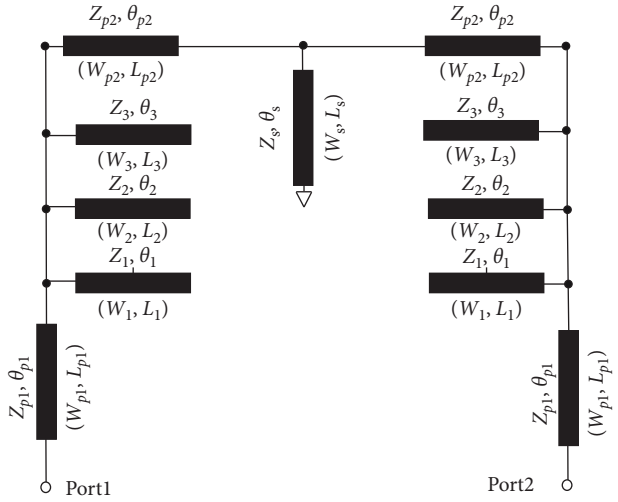

Figure 13: The equivalent transmission line model for the proposed sext-band BPF.

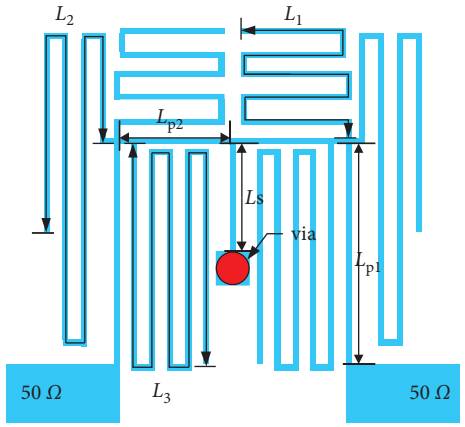

Figure 14: Structure of the proposed sext-band BPF.

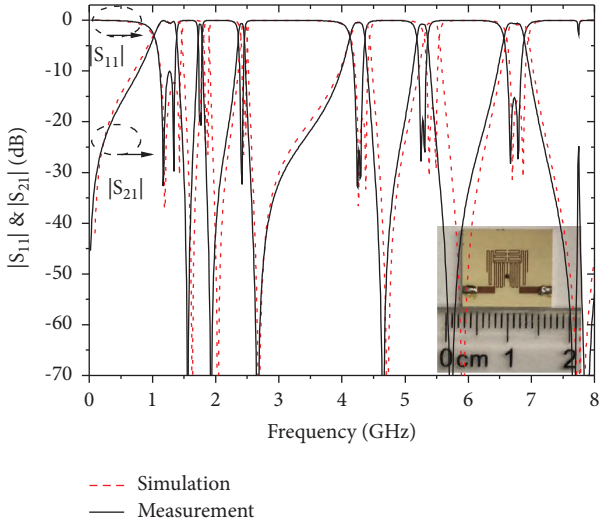

Figure 15: Simulated and measured results of sext-band BPF.

Table 1: Comparison with some previous multi-band BPFs.

Ref.	Frequency (GHz)	Insertion loss (dB)	Isolation (dB)	Size ($\lambda_g \times \lambda_g$)
[5]	1.48/2.49/3.47/4.49/5.78	1.49/1.78/0.89/1.18/2.47	ISO_{12}>34.77 ISO_{23}>27.91 ISO_{34}>32.98 ISO_{45}>30.88	0.24×0.17 (0.0408)
[6]	0.59/0.88/1.17/1.48/1.79	2.79/2.88/2.87/2.58/2.27	ISO_{12}>27.89 ISO_{23}>29.97 ISO_{34}>35.78 ISO_{45}>26.90	0.51×0.05 (0.0255)
[7]	0.88/1.19/1.37/1.66/1.97/2.39	2.28/1.99/2.27/2.68/2.19/1.97	ISO_{12}>37.98 ISO_{23}>19.87 ISO_{34}>29.80 ISO_{45}>21.92 ISO_{56}>14.85	0.26×0.15 (0.039)
[8]	0.69/1.98/3.18/4.49/5.77/6.95	1.29/0.58/0.79/1.06/1.37/2.16	ISO_{12}>52.83 ISO_{23}>44.95 ISO_{34}>51.72 ISO_{45}>41.92 ISO_{56}>37.88	0.16×0.09 (0.0144)
This work	**1.23/1.76/2.38/4.24/5.23/6.75**	**1.52/1.61/1.43/0.79/0.68/0.87**	**ISO_{12}>70.00 ISO_{23}>70.00 ISO_{34}>70.00 ISO_{45}>70.00 ISO_{56}>70.00**	**0.08×0.07 (0.0056)**

proposed sext -band BPF in this paper exhibits compact size, high selectivity, and a conveniently adjustable frequency response.

4. Conclusions

This paper presents miniaturized multiband BPFs by using a single multimode resonator loaded with branches. The proposed multiband BPFs feature very high design freedom for every single passband. The simulated and measured results have good agreement, which shows that the proposed filters feature compact size and high selectivity. Owing to these merits, the proposed structure could be a good candidate for multiband BPF design.

Data Availability

The data used in this study can be obtained free of charge form https://pan.baidu.com/s/1CbroDDVOh8nv4Y8uiUGlWQ?pwd=5axh.

Conflicts of Interest

The authors declare that they have no conflicts of interest.

Acknowledgments

This work was supported by the "Design of compact high performance MEMS filter," Chengdu Songyuan Photoelectric Technology Co., Ltd, China and the State Key Laboratory of Millimeter Waves (K202121), Southeast University, China.

References

[1] T. F. Yan, X. H. Tang, and J. Wang, "A novel quad-band bandpass filter using short stub loaded E-shaped resonators," *IEEE Microwave and Wireless Components Letters*, vol. 25, no. 8, pp. 508–510, 2015.

[2] D. Bukuru, K. Song, F. Zhang, Y. Zhu, and M. Fan, "Compact quad-band band pass filter using quad-mode stepped impedance resonator and multiple coupling circuits," *IEEE Transactions on Microwave Theory and Techniques*, vol. 65, no. 3, pp. 783–791, 2017.

[3] X. Li, Y. Zhang, Y. Tian, Y. Yang, and Y. Fan, "Quad- and sext-band bandpass filter based on multimode resonator utilizing SIRs loaded tapered line," *Microwave and Optical Technology Letters*, vol. 60, no. 3, pp. 650–654, 2018.

[4] A. Kamma, R. Das, and J. Mukherjee, "Spurious free independently controllable compact quad-band filter using folded T-shaped stub loaded modified ring resonator," *IET Microwaves, Antennas & Propagation*, vol. 11, no. 8, pp. 1156–1161, 2017.

[5] Y. Zhang, F. Ling, R. Huang, Z. Zhong, and B Zhang, "The characteristics of a terahertz filter with three-layer stacked structure," *Optik*, vol. 168, pp. 847–852, 2018.

[6] D. Li, Y. Yu, R. Song, M. Tang, J. Ai, and Y. Liao, "Design of compact quad-band bandpass filter with good selectivity using two-/tri-section SIRs and stepped impedance inverters," *IET Microwaves, Antennas & Propagation*, vol. 13, no. 5, pp. 675–682, 2019.

[7] W. Yang, L. Wang, and L. Wang, "Design of a quint-band bandpass filter based on multi-mode resonator," in *Proceedings of the 2021 IEEE International Conference on Power Electronics, Computer Applications (ICPECA)*, January 2021.

[8] H. Liu, R. Wang, and C. Lai, "A Compact Quint-Band Bandpass Filter with High Selectivity Using Uniform

Impedance Resonators (UIRs)," in *Proceedings of the 2020 IEEE MTT-S International Microwave Workshop Series on Advanced Materials and Processes for RF and THz Applications (IMWS-AMP)*, July 2020.

[9] K. W. Hsu, W. C. Hung, and W. H. Tu, "Compact quint-band microstrip bandpass fifilter using double-layered substrate," *IEEE International Microwave Symposium*, vol. 6, pp. 1–3, 2014.

[10] C. F. Chen, "Design of a compact microstrip quint-band fifilter based on the tri-mode stub-loaded stepped-impedance resonators," *IEEE Microwave and Wireless Components Letters*, vol. 22, pp. 357–359, 2012.

[11] K. W. Hsu, J. H. Lin, and W. H. Tu, "Compact sext-band bandpass filter with sharp rejection response," *IEEE Microwave and Wireless Components Letters*, vol. 24, no. 9, pp. 593–595, 2014.

[12] J. Ai, Y. H. Zhang, K. D. Xu, Y. J. Guo, W. T. Joines, and Q. H. Liu, "Compact sext-band bandpass filter based on single multimode resonator with high band-to-band isolations," *Electronics Letters*, vol. 52, no. 9, pp. 729–731, 2016.